Enhanced Cycling Stability of Lithium-Ion Batteries Using Graphene-Wrapped Fe3O4-Graphene Nanoribbons as Anode Materials

ARTICLE *in* ADVANCED ENERGY MATERIALS · MAY 2015

Impact Factor: 16.15 · DOI: 10.1002/aenm.201500171

10 AUTHORS, INCLUDING:

Lei Li
New York State Department of Health
31 PUBLICATIONS **586** CITATIONS
SEE PROFILE

Zhiwei Peng
University of Maryland, College Park
49 PUBLICATIONS **1,393** CITATIONS
SEE PROFILE

Nam Dong Kim
Rice University
43 PUBLICATIONS **653** CITATIONS
SEE PROFILE

Changsheng Xiang
Rice University
26 PUBLICATIONS **753** CITATIONS
SEE PROFILE

ADVANCED ENERGY MATERIALS
www.advenergymat.de

Enhanced Cycling Stability of Lithium-Ion Batteries Using Graphene-Wrapped Fe_3O_4-Graphene Nanoribbons as Anode Materials

*Lei Li, Anton Kovalchuk, Huilong Fei, Zhiwei Peng, Yilun Li, Nam Dong Kim, Changsheng Xiang, Yang Yang, Gedeng Ruan, and James M. Tour**

Rechargeable lithium-ion batteries (LIBs) are a remarkably practical and effective means for storing electrochemical energy.[1,2] LIBs have attracted significant interest given their use in a broad range of devices including electric vehicles and mobile communication technology.[3,4] With rapidly increasing demand for improved LIBs, the development of energy storage devices with high power density, energy density, and excellent cycling stability has become critical. To meet these demands, great effort has been devoted to develop superior electrode materials including using iron oxide (Fe_3O_4) which has attracted great interest due to its high theoretical reversible capacity (928 mAh g^{-1}), abundance, low cost, low toxicity, and eco-friendly properties.[1,5–9] However, the volume expansion and contraction during reversible discharge/charge processes leads to pulverization of Fe_3O_4 electrodes, resulting in fast capacity decay and poor cycle life. Therefore, development of Fe_3O_4-based anodes with high capacity and enhanced cycling stability is necessary.

To address these problems, various strategies have been developed to improve electrical conductivity while enhancing the structural stability of Fe_3O_4-based anode materials. One strategy is to prepare nanostructured materials that can relax the strain caused by the volume variation during discharge/charge processes and thereby improving the rate performance due to the short diffusion length of nanosized materials.[2,10] Nanomaterials prepared on different carbon substrates, such as carbon nanotubes,[11–14] graphene,[7,9,15–19] and amorphous carbon,[2,20,21] not only improve electrical conductivity but also mitigate volume variation, resulting in improved cycle stability of the composites. Another strategy is to use carbon coatings or encapsulation of the active materials to improve electrical conductivity and prevent aggregation of the actives.[2,7,22–26] However, since the cycling stability of Fe_3O_4-based anode materials is still reduced by pulverization of the active materials, preparation of Fe_3O_4-based anode materials with a specialized structure that prevents the negative effect of pulverization is still challenging and necessary.

In this study, we combined these design criteria into a hierarchical structured composite of the graphene-wrapped Fe_3O_4-graphene nanoribbons (G-Fe_3O_4-GNRs). In this composite, reduced graphene oxide and GNRs are in good electrical contact with the Fe_3O_4, which improves composite conductivity and also prevents loss of Fe_3O_4 caused by volume changes during discharge/charge processes, thus improving the overall electrochemical stability. More importantly, reduced graphene oxide is a softer coating layer when compared to other carbon coatings that are formed through calcinations or encapsulation of the active materials.[2,7,20] The soft graphene-based layer would alleviate the problems of having a more rigid carbon framework, which could not effectively release strain caused by volume changes. G-Fe_3O_4-GNRs as anode materials demonstrate high capacity, good rate performance, and improved cycling performance and are therefore a promising composite for use in LIBs.

The preparation of G-Fe_3O_4-GNRs is illustrated in **Scheme 1**. GNRs are a suitable template for loading Fe_3O_4 owing to their high specific surface area, electrical conductivity, and commercial scalability. GNRs were prepared using a previously described methodology that splits multiwalled carbon nanotubes in the presence of 1,2-dimethoxyethane (DME).[27] Fe_3O_4-GNRs were synthesized according to a multistep protocol, where $FeCl_3$ is loaded onto GNRs forming $FeCl_3$-GNRs, which is then reduced by Na/K alloy to form Fe-GNRs and finally oxidized to Fe_3O_4-GNRs under ambient conditions.[28] In order to increase the Fe_3O_4 content in the composite, a second intercalation step is performed by repeating steps (a)–(c) in Scheme 1. Next, Fe_3O_4-GNRs were dispersed in an aqueous solution of poly(diallyldimethylammoniumchloride) (PDADMAC) to form positively charged PDADMAC-Fe_3O_4-GNRs. Finally, G-Fe_3O_4-GNRs were obtained through electrostatic interaction between PDADMAC-Fe_3O_4-GNRs and reduced graphene oxide.[29–31] Reduced graphene oxide-Fe_3O_4 (G-Fe_3O_4), Fe_3O_4-reduced graphene oxide (Fe_3O_4-G), and Fe_3O_4-graphene oxide (Fe_3O_4-GO) as control samples were also prepared using the same procedures.

The morphologies of G-Fe_3O_4-GNRs, Fe_3O_4-GNRs, G-Fe_3O_4, Fe_3O_4-G, Fe_3O_4-GO, Fe_3O_4, and GNRs were studied by scanning

Dr. L. Li, Dr. A. Kovalchuk, Dr. H. Fei, Dr. Z. Peng, Y. Li, Dr. N. D. Kim, Dr. C. Xiang, Dr. Y. Yang, Dr. G. Ruan, Prof. J. M. Tour
Department of Chemistry
Rice University
6100 Main Street, Houston, TX 77005, USA
E-mail: tour@rice.edu
Y. Yang, J. M. Tour
Smalley Institute for Nanoscale Science and Technology
Rice University
6100 Main Street, Houston, TX 77005, USA
J. M. Tour
Department of Materials Science and Nano Engineering
Rice University
6100 Main Street, Houston, TX 77005, USA

DOI: 10.1002/aenm.201500171

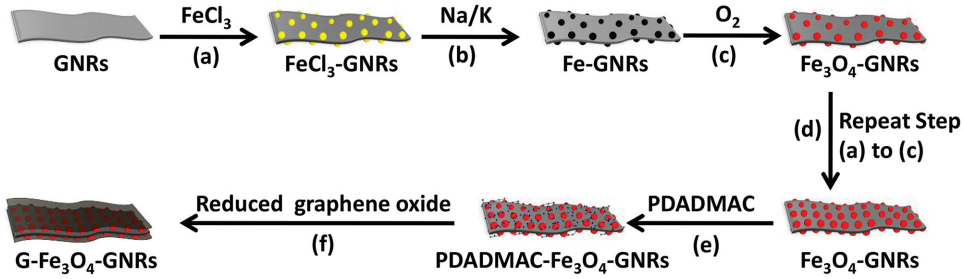

Scheme 1. Schematic illustration of the synthesis of G-Fe_3O_4-GNRs.

electron microscopy (SEM) and transmission electron microscopy (TEM). **Figure 1**a,b shows SEM images of Fe_3O_4-GNRs at different magnifications where Fe_3O_4 had grown around GNRs (Figure S1a,b, Supporting Information). Figure 1c shows a TEM image of one strip of Fe_3O_4-GNRs, where Fe_3O_4 nanoparticles have uniformly coated the GNR surface. High resolution TEM imaging of Fe_3O_4-GNRs (Figure 1d) shows that the diameter of Fe_3O_4 nanoparticles is ≈10 nm. Without GNRs, Fe_3O_4 is consistent with different size particles and flakes as shown in Figure S1c,d (Supporting Information), demonstrating GNRs induce the formation of uniform Fe_3O_4 nanoparticles. Figure S1e,f (Supporting Information) shows SEM images of G-Fe_3O_4 at different magnifications, indicating Fe_3O_4 is in reduced graphene oxide. TEM images of G-Fe_3O_4 further show the Fe_3O_4 in the form of nanoparticles and flakes in reduced graphene oxide (Figure S1g,h, Supporting Information). Figure S1i,j (Supporting Information) shows SEM images of Fe_3O_4-G at different magnifications indicating Fe_3O_4 in graphene, which is further confirmed by TEM images in Figure S1k,l (Supporting Information). Fe_3O_4-GO demonstrates the similar morphology as shown in Figure S1m–p (Supporting Information). Figure 1e shows an SEM image of G-Fe_3O_4-GNRs, where reduced graphene oxide serves as a binder to connect the separated Fe_3O_4-GNRs together forming the entirety of G-Fe_3O_4-GNRs. The ribbon-like morphology of Fe_3O_4-GNRs was still observed within G-Fe_3O_4-GNRs (Figure 1f).

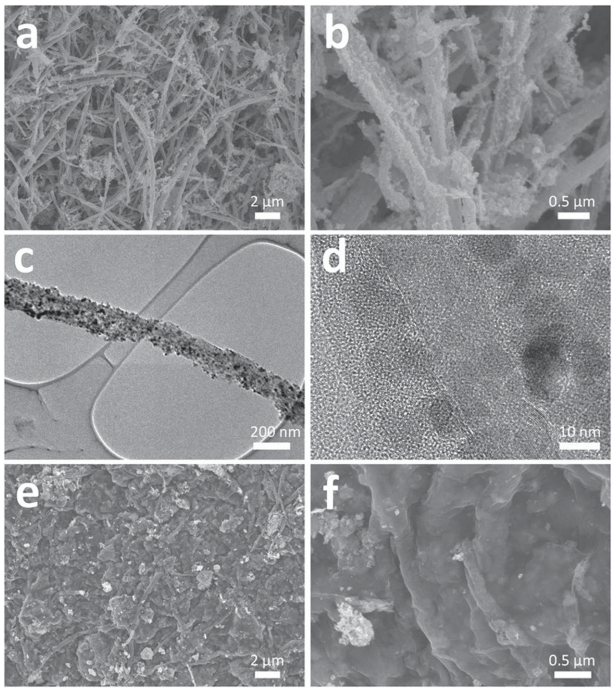

Figure 1. a,b) SEM images of Fe_3O_4-GNRs at different magnifications. c,d) TEM images of Fe_3O_4-GNRs at different magnifications. e,f) SEM images of G-Fe_3O_4-GNRs at different magnifications.

The composites were also studied by X-ray diffraction (XRD) and X-ray photoelectron spectroscopy (XPS). **Figure 2**a shows XRD patterns of GNRs, Fe_3O_4-GNRs, and G-Fe_3O_4-GNRs revealing that the peak of GNRs at 26.5° results from graphite diffraction peak (002) and the iron oxide growing from GNRs is Fe_3O_4.[23,32–35] The characteristic peaks of Fe_3O_4 and GNRs are clearly observed in the XRD patterns of Fe_3O_4-GNRs and G-Fe_3O_4-GNRs. Figure 2b shows the XPS spectrum of G-Fe_3O_4-GNRs revealing that the composite contains Fe, C, and O with trace amounts of N from hydrazine adducts introduced with the reduced graphene oxide and compared to the survey XPS spectra of composite Fe_3O_4-GNRs in Figure S2a (Supporting Information) shows no N content. The two characteristic peaks of Fe2p3/2 and Fe2p1/2 depicted in the fine spectra of Fe2p are centered at 711 and 725 eV, confirming the formation of Fe_3O_4 in the composite (Figures 2c and S2b, Supporting Information), hence the graphene coating process did not change the electronic state of Fe_3O_4.[36,37] Figure 2d shows the fine XPS spectra of C1s of G-Fe_3O_4-GNRs with four peaks located at 284.5, 285.5, 286.4, and 287.4 eV, assigned to C=C/C–C, C–O, C=O, and O–C=O, respectively.[38–40] The analysis of C1s of G-Fe_3O_4-GNRs shows that the graphene oxide was not completely reduced by hydrazine. After graphene wrapping, the Fe_3O_4 content decreased from 79% to 60% (Figure S3a,b, Supporting Information). G-Fe_3O_4, Fe_3O_4-G, and Fe_3O_4-GO as control samples show 53%, 55%, and 71% Fe_3O_4 content, respectively (Figure S3c–e, Supporting Information).

The electrochemical performance of G-Fe_3O_4-GNRs as anodes in LIBs were studied using cyclic voltammetry (CV) and discharge/charge experiments. As shown in **Figure 3**a, there were three cathodic peaks at 1.47, 0.73, and 0.50 V in the first CV cycle. The peak at 1.47 V resulted from the structure transition caused by lithium interaction with crystalline Fe_3O_4, as shown in the equation ($Fe_3O_4 + xLi^+ + xe^- \rightleftharpoons Li_x(Fe_3O_4)$ $(0 \le x \le 2)$). The peak at 0.73 V corresponded to further reduction of $Li_x(Fe_3O_4)$ to Fe(0) as shown in the equation of $Li_x(Fe_3O_4) + (8-x)Li^+ + (8-x)e^- \rightleftharpoons 3Fe + 4Li_2O (0 \le x \le 2)$.[11,41–43] The peak at 0.50 V resulted from the formation of the solid electrolyte interface (SEI) which occurs during the first cycle but disappears in the subsequent cycles. Two anode peaks at 1.69 and

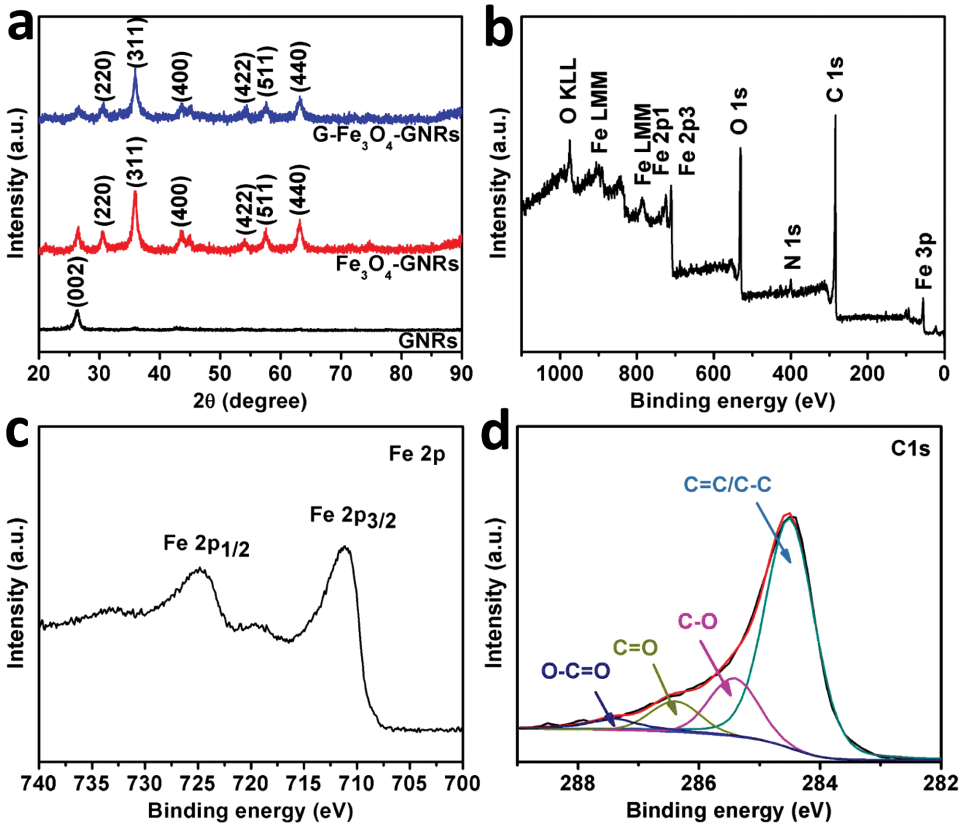

Figure 2. a) XRD patterns of GNRs, Fe_3O_4-GNRs, and G-Fe_3O_4-GNRs. b) XPS spectrum of G-Fe_3O_4-GNRs. c) Fe2p XPS spectrum of G-Fe_3O_4-GNRs. d) XPS spectrum of C 1s for G-Fe_3O_4-GNRs.

2.00 V correspond to the gradual oxidation of Fe(0) to $Li_x(Fe_3O_4)$ and Fe^{3+} in two steps during the CV cycle, respectively. After the first cycle, the CV curves nearly overlap in subsequent cycles, indicating good reversibility of the samples, as do the CV curves in Figure S4 (Supporting Information) for Fe_3O_4-GNRs and GNRs. This was further studied by the discharge/charge profiles of G-Fe_3O_4-GNRs at 0.1 A g^{-1}, as shown in Figure 3b, where there is a plateau at ≈0.80 V in the discharge process and a plateau with two transitions at ≈1.5 and 2.0 V in the charge process, which is consistent with peaks in the corresponding CV curves. Fe_3O_4-GNRs, G-Fe_3O_4, Fe_3O_4-G, and Fe_3O_4-GO display similar phenomena (Figure S4a–h, Supporting Information). Figure S4i,j (Supporting Information) shows the CV and charge discharge curves of GNRs. All the discharge capacities of GNRs, Fe_3O_4-GO, Fe_3O_4-G, G-Fe_3O_4, Fe_3O_4-GNRs, and G-Fe_3O_4-GNRs had a great loss in the second cycle compared to the first cycle likely due to the formation of SEI, the irreversible reaction of the electrodes, and the decomposition of electrolyte.[11,20]

The rate and cycling performance of G-Fe_3O_4-GNRs were also evaluated by extended discharge/charge experiments. **Figure 4**a shows the capacity of G-Fe_3O_4-GNRs which exhibited no decay at different current densities. For example, the discharge capacity was 787 mAh g^{-1} at the 30th cycle and 796 mAh g^{-1} at the 55th cycle at 0.1 A g^{-1}. These results demonstrate the good rate performance of G-Fe_3O_4-GNRs. After 55 cycles of rate testing, the morphology of G-Fe_3O_4-GNRs has no obvious change as shown in Figure S5 (Supporting Information). Figure 4b compares the cycling stability of G-Fe_3O_4-GNRs, Fe_3O_4-GNRs, G-Fe_3O_4, Fe_3O_4-G, Fe_3O_4-GO, and GNRs in LIBs in the same potential window. GNRs showed a very low, yet stable discharge capacity that increased little from an initial value of 172 mAh g^{-1} at the second cycle to 186 mAh g^{-1} by the 100th cycle. Fe_3O_4-GNR,

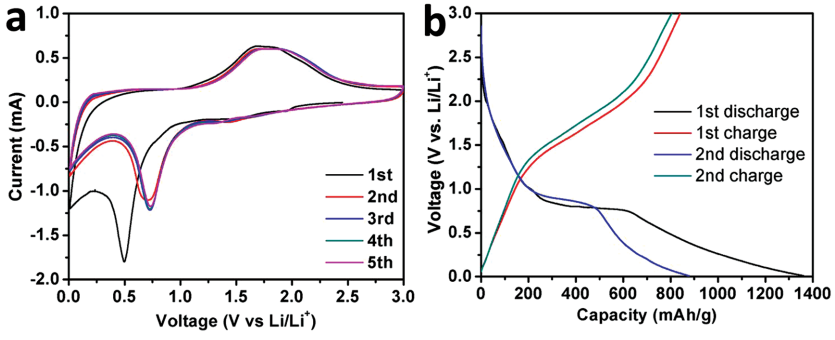

Figure 3. a) Cyclic voltammetry curves of G-Fe_3O_4-GNRs in the potential range of 0.01 and 3.0 V (vs Li/Li^+) at a scan rate of 0.4 mV s^{-1}. b) The first two discharge charge curves of G-Fe_3O_4-GNRs in the potential range of 0.01 and 3.0 V (vs Li/Li^+) at a current density of 0.1 A g^{-1}.

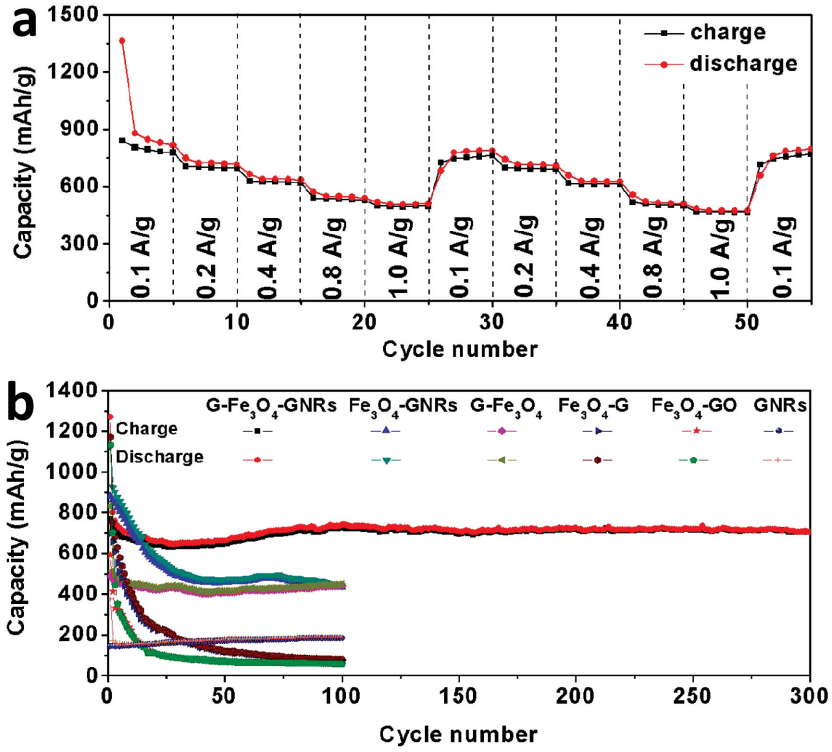

Figure 4. a) Rate performance of G-Fe_3O_4-GNRs at various current rates from 0.1 to 1.0 A g^{-1} in the potential range of 0.01 and 3.0 V (vs Li/Li^+). b) Cycling performance of G-Fe_3O_4-GNRs, Fe_3O_4-GNRs, G-Fe_3O_4, Fe_3O_4-G, Fe_3O_4-GO, and GNRs at a current density of 0.4 A g^{-1} and potential range of 0.01 and 3.0 V (vs Li/Li^+).

Fe_3O_4-G, and Fe_3O_4-GO electrodes exhibited a sharp decline in discharge capacity from 926, 752, and 703 mAh g^{-1} in the second cycle to 544, 211, and 95 mAh g^{-1} by the 25th cycle and finally only 442, 77, and 57 mAh g^{-1} by the 100th cycle, respectively. G-Fe_3O_4 electrodes show the low discharge capacity and gradually decreased from 513 mAh g^{-1} at the second cycle to 447 mAh g^{-1} at the 100th cycle. However, after graphene wrapping of Fe_3O_4-GNR, the discharge capacity of G-Fe_3O_4-GNRs slowly decreased from 800 mAh g^{-1} at the second cycle to 652 mAh g^{-1} at the 25th cycle and then rose to 740 mAh g^{-1} at the 100th cycle and reached a stable capacity of 708 mAh g^{-1} after 300 cycles. More importantly, Coulombic efficiency of G-Fe_3O_4-GNRs was maintained ≈99.5%, excluding the first several cycles (Figure S6, Supporting Information). This material showed competitive performance, especially in cycling performance compared to the reported works (Table S1, Supporting Information). Therefore, these results demonstrated that the unique hierarchical structure effectively reduced the capacity decay and greatly improved the capacity and cycling stability of G-Fe_3O_4-GNRs.

Electrochemical impedance spectroscopy experiments were carried out to further study the enhanced electrochemical performance of G-Fe_3O_4-GNRs (**Figure 5**a). An equivalent circuit model for this system was established as shown in Figure 5b. In this model, R_s is the internal resistance of the tested battery, R_{SEI} and R_{ct} represent the SEI surface and charge-transfer resistance, CPE_1 and CPE_2 are associated with constant phase element, Z_w is the Warburg resistance related to the lithium diffusion process, and the C_{int} is the interaction capacitance.[45] In the Figure 5a, the plots consist of two semicircles in the high and intermediate frequency range, which result from the Li^+ ion transport through the SEI film (R_{SEI}) and the interfacial charge transfer reaction (R_{ct}) combined with CPE_1 and CPE_2, respectively. They also have a sloping line because of the solid-state Li diffusion into the active materials (Z_w).[45,46] Table S2 (Supporting Information) showed the fitted impedance parameters based on the experimental Nyquist plots using the established model in Figure 5b. Both R_{SEI} (32 Ω) and R_{ct} (9.6 Ω) of G-Fe_3O_4-GNRs are lower than that of Fe_3O_4-GNRs (R_{SEI} = 47 Ω and R_{ct} = 21 Ω), G-Fe_3O_4 (R_{SEI} = 73 Ω and R_{ct} = 35 Ω), Fe_3O_4-G (R_{SEI} = 52 Ω and R_{ct} = 53 Ω), and Fe_3O_4-GO (R_{SEI} = 46 Ω and R_{ct} = 97 Ω), which means G-Fe_3O_4-GNRs have a more stable surface film and faster charge transfer process than the other control samples.[46] It indicates that incorporation of graphene and GNRs on G-Fe_3O_4-GNRs can greatly improve its electrical conductivity and mechanical stability, resulting in significant improvement in the electrochemical performance.

In summary, a nanoscale sandwiched composite of graphene-wrapped Fe_3O_4-graphene nanoribbons was successfully designed and synthesized. In this composite, graphene tightly sandwiched the nanosized Fe_3O_4 which grew directly on the GNRs. G-Fe_3O_4-GNRs demonstrate high capacity, good rate

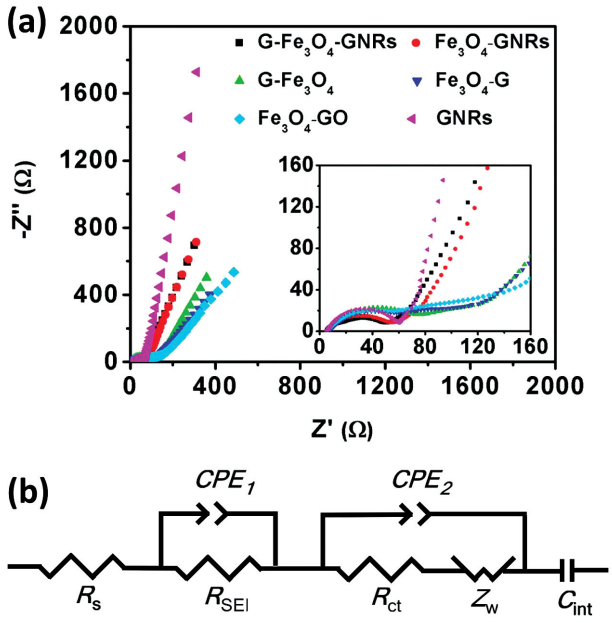

Figure 5. a) Nyquist plots of G-Fe_3O_4-GNRs, Fe_3O_4-GNRs, G-Fe_3O_4, Fe_3O_4-G, Fe_3O_4-GO, and GNRs. The inset is the enlarged high frequency region. b) Equivalent circuit that is used to fit the experimental data.

performance, and improved cycling stability as anode materials due to the synergy between Fe_3O_4, graphene, and GNRs. The design concept developed here provides a flexible system to mitigate the effects of oxide pulverization while permitting facile ion access to the nanostructures, opens up a new avenue for constructing anodes with improved electrochemical stability for lithium-ion batteries.

Experimental Section

Synthesis of Fe_3O_4-GNRs: GNRs were prepared by splitting multiwalled carbon nanotubes with Na/K in DME and quenching of the reaction with MeOH as described previously.[27] Fe_3O_4-GNRs were synthesized according to the multistep protocol. Two intercalation steps are needed to achieve high content of Fe_3O_4 in the composite. The Fe_3O_4-GNRs were synthesized by adding 100 mg of GNRs and 300 mg of $FeCl_3$ to a glass ampule that was sealed under vacuum using an acetylene torch. The ampule was placed in an oven at 350 °C for 24 h to afford intercalation of the $FeCl_3$ into the GNRs. The $FeCl_3$-GNRs were transferred into around bottom glass flask (250 mL), sealed, and carefully purged with nitrogen. Next, 35 mL of freshly distilled DME and 1 mL of Na/K alloy were added to the flask and the mixture solution was stirred for 15 h at room temperature. The reaction was quenched with 30 mL of methanol and then carefully filtered (Sartorius Stedim Biotech, polytetrafluorethylene (PTFE), pore size 5 μm) by vacuum filtration and washed with deionized (DI) water, methanol, acetone, and diethyl ether and dried under vacuum (≈7 mmHg) at 100 °C for 24 h. A 426 mg of this product was placed in a glass ampule with 600 mg of $FeCl_3$, sealed under vacuum and placed at 350 °C in an oven for 24 h for final intercalation. 35 mL of DME and 1.2 mL Na/K alloy were carefully added and reacted at room temperature with stirring for 20 h. 30 mL of methanol was added to quench the reaction mixture. 778 mg of Fe_3O_4-GNRs was collected by drying under vacuum (≈7 mm Hg) at 100 °C for 24 h after vacuum filtration and washing with water, methanol, acetone, and diethyl ether. Fe_3O_4-G, Fe_3O_4-GO, and Fe_3O_4 were prepared using the same procedure without the addition of GNRs.

Synthesis of G-Fe_3O_4-GNRs: 70 mg of Fe_3O_4-GNRs was dispersed in 70 mL of DI water containing 0.7 mL of poly(diallyldimethylammonium chloride) (PDADMAC, Sigma-Aldrich) by ultrasonication (Cole-Parmer Instrument Company, 17 W). After stirring for 5 h at room temperature, 62 mg of PDADMAC-Fe_3O_4-GNRs was obtained via vacuum filtration and washing with 500 mL of DI water, 100 mL of ethanol, and then drying under vacuum (≈7 mmHg) at 80 °C for 10 h. Next, 60 mg of PDADMAC-Fe_3O_4-GNRs was dispersed in 60 mL of DI water, which was adjusted to pH 8 by ammonia (1 M, CH_3CH_2OH). Reduced graphene oxide was synthesized by reduction of 30 mg of graphene oxide in 60 mL of DI water (pH 8, ammonia) with 33.9 μL of hydrazine. The PDADMAC-Fe_3O_4-GNRs suspension was mixed with reduced graphene oxide and the solution was stirred for 5 h. 60 mg of G-Fe_3O_4-GNRs was collected by drying under vacuum (≈7 mmHg) at 80 °C for 10 h after vacuum filtration and washing with 500 mL of DI water and 100 mL of ethanol. G-Fe_3O_4 was prepared using the same method as above.

Materials Characterization: Products were characterized by SEM (JEOL 6500), TEM (JEM2100F TEM), XRD (Rigaku D/Max Ultima II), XPS (PHI Quantera), and TGA (TA Instruments, Q50).

Electrochemical Measurements: The lithium-ion batteries were assembled using the same procedure as described previously.[46] CV experiments were carried out on a CHI660D and galvanostatic discharge/charge tests were carried out on a LANDCT2001A battery system. Capacity values were based on the total mass of the active composite.

Supporting Information

Supporting Information is available from the Wiley Online Library or from the author.

Acknowledgements

Sandia National Laboratory, the Air Force Office of Sponsored Research (AFOSR) Multidisciplinary University Research Initiative (MURI) program (FA9550-12-1-0035), the AFOSR (FA9550-14-1-0111), the Office of Naval Research MURI program (Grant Nos. 00006766 and N00014-09-1-1066), and the Chinese scholarship council provided funding. The authors would also like to thank Celgard LLC for the kind donation of the battery separator material (Celgard 2300).

Received: January 23, 2015
Revised: April 19, 2015
Published online:

[1] V. Etacheri, R. Marom, R. Elazari, G. Salitra, D. Aurbach, *Energy Environ. Sci.* **2011**, *4*, 3243.
[2] J. E. Lee, S. H. Yu, D. J. Lee, D. C. Lee, S. I. Han, Y. E. Sung, T. Hyeon, *Energy Environ. Sci.* **2012**, *5*, 9528.
[3] J. M. Tarascon, M. Armand, *Nature* **2001**, *414*, 359.
[4] B. Wang, X. Li, X. Zhang, B. Luo, M. Jin, M. Liang, S. A. Dayeh, S. T. Picraux, L. Zhi, *ACS Nano* **2013**, *7*, 1437.
[5] A. S. Aricò, P. Bruce, B. Scrosati, J. M. Tarascon, W. Schalkwijk, *Nat. Mater.* **2005**, *4*, 366.
[6] M. V. Reddy, G. V. Subba Rao, B. V. R. Chowdari, *Chem. Rev.* **2013**, *113*, 5364.
[7] G. Zhou, D. W. Wang, F. Li, L. Zhang, N. Li, Z. S. Wu, L. Wen, G. Q. Lu, H. M. Cheng, *Chem. Mater.* **2010**, *22*, 5306.
[8] W. M. Zhang, X. L. Wu, J. S. Hu, Y. G. Guo, L. J. Wan, *Adv. Funct. Mater.* **2008**, *18*, 3941.
[9] W. Wei, S. Yang, H. Zhou, I. Lieberwirth, X. Feng, K. Müllen, *Adv. Mater.* **2013**, *25*, 2909.
[10] P. G. Bruce, B. Scrosati, J. M. Tarascon, *Angew. Chem. Int. Ed.* **2008**, *47*, 2930.
[11] X. Jia, Z. Chen, X. Cui, Y. Peng, X. Wang, G. Wang, F. Wei, Y. Lu, *ACS Nano* **2012**, *6*, 9911.
[12] J. Cheng, B. Wang, C. M. Park, Y. Wu, H. Huang, F. Nie, *Chem. Eur. J.* **2013**, *19*, 9866.
[13] Y. Wu, Y. Wei, J. Wang, K. Jiang, S. Fan, *Nano Lett.* **2013**, *13*, 818.
[14] J. Liu, J. Ni, Y. Zhao, H. Wang, L. Gao, *J. Mater. Chem. A* **2013**, *1*, 12879.
[15] F. Zhang, T. Zhang, X. Yang, L. Zhang, K. Leng, Y. Huang, Y. Chen, *Energy Environ. Sci.* **2013**, *6*, 1623.
[16] D. Chen, H. Quan, J. Liang, L. Guo, *Nanoscale* **2013**, *5*, 9684.
[17] L. Zhuo, Y. Wu, L. Wang, J. Ming, Y. Yu, X. Zhang, F. Zhao, *J. Mater. Chem. A* **2013**, *1*, 3954.
[18] Y. Dong, R. Ma, M. Hu, H. Cheng, Q. Yang, Y. Y. Li, J. A. Zapien, *Phys. Chem. Chem. Phys.* **2013**, *15*, 7174.
[19] Y. Chen, B. Song, L. Lu, J. Xue, *Nanoscale* **2013**, *5*, 6797.
[20] C. He, S. Wu, N. Zhao, C. Shi, E. Liu, J. Li, *ACS Nano* **2013**, *7*, 4459.
[21] L. Wang, J. Liang, Y. Zhu, T. Mei, X. Zhang, Q. Yang, Y. Qian, *Nanoscale* **2013**, *5*, 3627.
[22] G. Derrien, J. Hassoun, S. Panero, B. Scrosati, *Adv. Mater.* **2007**, *19*, 2336.
[23] L. Li, A. R. O. Raji, J. M. Tour, *Adv. Mater.* **2013**, *25*, 6298.
[24] Y. S. Hu, R. Demir-Cakan, M. M. Titirici, J.-O. Müller, R. Schlögl, M. Antonietti, J. Maier, *Angew. Chem. Int. Ed.* **2008**, *47*, 1645.

[25] X. W. Lou, J. S. Chen, P. Chen, L. A. Archer, *Chem. Mater.* **2009**, *21*, 2868.
[26] L. Wang, Y. Yu, P. C. Chen, D. W. Zhang, C. H. Chen, *J. Power Sources* **2008**, *183*, 717.
[27] B. Genorio, W. Lu, A. M. Dimiev, Y. Zhu, A. R. O. Raji, B. Novosel, L. B. Alemany, J. M. Tour, *ACS Nano* **2012**, *6*, 4231.
[28] B. Genorio, Z. Peng, W. Lu, B. K. Price Hoelscher, B. Novosel, J. M. Tour, *ACS Nano* **2012**, *6*, 10396.
[29] D. Li, M. B. Muller, S. Gilje, R. B. Kaner, G. G. Wallace, *Nat. Nanotechnol.* **2008**, *3*, 101.
[30] D. C. Marcano, D. V. Kosynkin, J. M. Berlin, A. Sinitskii, Z. Sun, A. Slesarev, L. B. Alemany, W. Lu, J. M. Tour, *ACS Nano* **2010**, *4*, 4806.
[31] Z. Lei, F. Shi, L. Lu, *ACS Appl. Mater. Interfaces* **2012**, *4*, 1058.
[32] J. Campos-Delgado, J. M. Romo-Herrera, X. Jia, D. A. Cullen, H. Muramatsu, Y. A. Kim, T. Hayashi, Z. Ren, D. J. Smith, Y. Okuno, T. Ohba, H. Kanoh, K. Kaneko, M. Endo, H. Terrones, M. S. Dresselhaus, M. Terrones, *Nano Lett.* **2008**, *8*, 2773.
[33] S. H. Lee, S. H. Yu, J. E. Lee, A. Jin, D. J. Lee, N. Lee, H. Jo, K. Shin, T. Y. Ahn, Y.-W. Kim, H. Choe, Y.-E. Sung, T. Hyeon, *Nano Lett.* **2013**, *13*, 4249.
[34] Y. Shi, Y. Qiao, H. Chen, *Nanotechnology* **2012**, *23*, 395601.
[35] N. Zhao, S. Wu, C. He, Z. Wang, C. Shi, E. Liu, J. Li, *Carbon* **2013**, *57*, 130.
[36] Z. S. Wu, S. Yang, Y. Sun, K. Parvez, X. Feng, K. Müllen, *J Am. Chem. Soc.* **2012**, *134*, 9082.
[37] J. Su, M. Cao, L. Ren, C. Hu, *J. Phys. Chem. C* **2011**, *115*, 14469.
[38] S. Yang, W. Yue, J. Zhu, Y. Ren, X. Yang, *Adv. Funct. Mater.* **2013**, *23*, 3570.
[39] S. Utsumi, H. Honda, Y. Hattori, H. Kanoh, K. Takahashi, H. Sakai, M. Abe, M. Yudasaka, S. Iijima, K. Kaneko, *J. Phys. Chem. C* **2007**, *111*, 5572.
[40] S. Some, Y. Kim, Y. Yoon, H. Yoo, S. Lee, Y. Park, H. Lee, *Sci. Rep.* **2013**, *3*, 1929.
[41] F. Xu, W. Kang, X. Wang, R. Liu, C. Zhao, Q. Shen, *CrystEngComm* **2013**, *15*, 4431.
[42] X. Zhu, Y. Zhu, S. Murali, M. D. Stoller, R. S. Ruoff, *ACS Nano* **2011**, *5*, 3333.
[43] Z. Wang, D. Luan, S. Madhavi, Y. Hu, X. W. Lou, *Energy Environ. Sci.* **2012**, *5*, 5252.
[44] M. S. Wu, P. C. Chiang, J. C. Lin, *J. Electrochem. Soc.* **2005**, *152*, A47.
[45] G. M. Zhou, D. W. Wang, L. C. Yin, N. Li, F. Li, H. M. Cheng, *ACS Nano* **2012**, *6*, 3214.
[46] L. Li, A. Kovalchuk, J. M. Tour, *Nano Res.* **2014**, *7*, 1319.